

# mmCLIP: Boosting mmWave-based Zero-shot HAR via Signal-Text Alignment

Qiming Cao<sup>1</sup>, Hongfei Xue<sup>2\*</sup>, Tianci Liu<sup>1</sup>, Xingchen Wang<sup>1</sup>, Haoyu Wang<sup>1</sup>

Xincheng Zhang<sup>1</sup>, Lu Su<sup>1\*</sup>

<sup>1</sup>Purdue University, <sup>2</sup>The University of North Carolina at Charlotte

Email: <sup>1</sup>{cao393, liu3351, wang2930, wang5346, zhan5104, lusu}@purdue.edu, <sup>2</sup>hongfei.xue@charlotte.edu

## ABSTRACT

Millimeter-wave (mmWave) based human activity recognition (HAR) systems have demonstrated promising performance in various applications, leveraging the power of deep neural networks. However, these systems are suffering from the scarcity of available mmWave data for model training. To address this challenge, we explore the possibility of transferring knowledge from large AI models built on massive text and visual data to enhance the generalizability of mmWave-based HAR models. Towards this end, we introduce mmCLIP, a novel system that aligns mmWave signal space and text space to facilitate zero-shot recognition for unseen activities. To enable this alignment, we employ cross-modality signal synthesis to augment mmWave signal data using large human mesh datasets and design an activity attribute decomposition and recombination approach to characterize the semantic interconnections among activities. We conducted extensive experiments to demonstrate the effectiveness of our proposed framework.

## CCS CONCEPTS

- Human-centered computing → Ubiquitous and mobile computing;
- Computer systems organization → Embedded and cyber-physical systems.

## KEYWORDS

Wireless Sensing, mmWave, Human Activity Recognition, Signal Augmentation, Visual-Language Model, Large Language Model

### ACM Reference Format:

Qiming Cao<sup>1</sup>, Hongfei Xue<sup>2\*</sup>, Tianci Liu<sup>1</sup>, Xingchen Wang<sup>1</sup>, Haoyu Wang<sup>1</sup>, Xincheng Zhang<sup>1</sup>, Lu Su<sup>1\*</sup>. 2024. mmCLIP: Boosting mmWave-based Zero-shot HAR via Signal-Text Alignment. In *ACM Conference on Embedded Networked Sensor Systems (SenSys '24)*, November 4–7, 2024, Hangzhou, China. ACM, New York, NY, USA, 14 pages. <https://doi.org/10.1145/3666025.3699331>

## 1 INTRODUCTION

With the rising quest for intelligent systems that enhance human life, human activity recognition (HAR) plays a pivotal element in

---

\*Hongfei Xue and Lu Su are corresponding authors.

Permission to make digital or hard copies of all or part of this work for personal or classroom use is granted without fee provided that copies are not made or distributed for profit or commercial advantage and that copies bear this notice and the full citation on the first page. Copyrights for components of this work owned by others than the author(s) must be honored. Abstracting with credit is permitted. To copy otherwise, or republish, to post on servers or to redistribute to lists, requires prior specific permission and/or a fee. Request permissions from [permissions@acm.org](mailto:permissions@acm.org).

SenSys '24, November 4–7, 2024, Hangzhou, China

© 2024 Copyright held by the owner/author(s). Publication rights licensed to ACM.

ACM ISBN 979-8-4007-0697-4/24/11  
<https://doi.org/10.1145/3666025.3699331>

understanding human behavior, which enables a wide spectrum of applications ranging from healthcare [47, 50, 51] and surveillance [20, 35, 41] to smart homes [2, 38, 45] and human-computer interactions [31]. A variety of sensors can be utilized for HAR tasks, including cameras, wearable devices, and wireless signals. Among them, mmWave has emerged as a particularly advantageous sensing solution due to its low-cost and high-resolution nature.

However, the generalizability of the mmWave-based HAR remains constrained. The current implementations of mmWave-based HAR are predominantly tailored for specific, narrowly defined classification tasks, limiting their ability to identify activities beyond their initial training scope. This limitation primarily arises from the insufficiency of available mmWave sensing data, since the data collection process for mmWave-based HAR is laborious and time-intensive, requiring specialized hardware and software, significant participant engagement, as well as meticulous synchronization and calibration processes. These stringent requirements render large-scale data collection both financially and logically prohibitive. Consequently, researchers are often limited to collecting customized small datasets for their specific tasks, thereby impeding the advancement of generalizable mmWave-based HAR systems.

In recent years, we have witnessed remarkable advancements in the field of artificial intelligence (AI), particularly in natural language processing (NLP) [4, 8, 10, 44] and computer vision (CV) [37, 43, 55]. The cornerstone of these successes lies in the utilization of large datasets and expansive models. Scaling laws [24] have underscored this paradigm, demonstrating that the synergistic combination of big data and large models yields great generalizability. *Given these achievements, a fundamental question arises: Is it possible to transfer the knowledge in large AI models built upon massive text and visual data to elevate the generalizability of mmWave-based HAR models?*

To answer this question, we introduce mmCLIP, a novel framework designed to harness the knowledge embedded in extensive computer vision datasets and large language models to perform mmWave-based zero-shot HAR tasks. The main idea of our approach is to align the high-level representation space of mmWave signals with the text semantic space of pre-trained large language models (LLMs), enabling the framework to leverage the generalizability of these language models for predicting unseen activities. However, achieving accurate alignment between these two embedding spaces necessitates a substantial volume of paired signal-text data with diverse activity samples – a dataset that is neither readily available nor feasible to collect manually. To address this challenge, we propose leveraging cross-modality signal synthesis to augment mmWave signal data from the large human mesh datasets with text descriptions, thereby facilitating knowledge transfer from visual

data. This strategy allows us to generate an extensive synthetic paired dataset, which can be employed to pre-train our model. Then, we fine-tune the model by collecting a smaller set of real-world data to bridge the simulation-to-reality gap.

Another challenge is that directly aligning the signal data to the original text label space may not be able to yield satisfactory generalization results, as the text labels in many cases cannot precisely characterize human activities and thus may fail to capture the subtle relationships among different activities. For example, the activities “drink water” and “pick up an object” appear quite different from a text label perspective due to the distinct words used. However, the movements of limbs and torso involved in these activities are very similar. To capture such similarity, in our model, we introduce an activity attribute decomposition and recombination approach. For instance, during the activity of “sit down”, an individual will “bend his/her legs”, “keep his/her arms slightly bent forward”, and “remain stationary”. In this description, we describe the “legs status”, “arms status”, and “location status” of the subject performing the activity, regarding these statuses as distinct attributes of the activity. In our model design, we leverage the knowledge embedded in the LLMs to decompose the text label into attribute descriptions and further into text attribute embeddings. In this way, we can characterize the semantic relations among activities, represented as the similarities of their attribute embeddings. Returning to the example of “drink water” and “pick up an object,” from an attribute perspective, these two activities share similar descriptions and therefore have high embedding similarity. This allows the model to capture the relationship between them. On the other hand, mmWave signals can also characterize human activities by capturing activity attributes such as the movements of limbs and torso. In summary, our model explicitly extracts activity attributes from both signal and text space, allowing for a more nuanced and accurate representation of activities and their semantic interconnections.

We conclude the contributions of our paper as follows:

- We propose the mmCLIP framework which aligns the signal and text embedding space to achieve mmWave-based unseen activity recognition, where the model has never been trained on either the mmWave signal data or the exact text label of the unseen activities.
- We employ cross-modality signal synthesis to augment mmWave signal data using large human mesh datasets with text descriptions, thereby expanding the representation of human activities in signal space. We design an activity attribute decomposition and recombination approach to characterize human activities from the attribute level, reinforcing the semantic interconnections among activities as well as the alignment of signal and text space.
- To evaluate the proposed mmCLIP framework, we constructed a real-world human activity recognition testbed using commercial off-the-shelf (COTS) mmWave devices.
- Our evaluation results demonstrate that the mmCLIP system achieved an average accuracy of 76.4% on ten-class zero-shot classification tasks, highlighting the effectiveness of the mmCLIP framework for zero-shot HAR tasks.

## 2 SYSTEM OVERVIEW

The goal of our proposed mmCLIP framework is to develop an mmWave-based zero-shot human activity recognition system. Unlike conventional activity classifiers that predict the probability distribution over a fixed set of predetermined classes, mmCLIP aligns the high-level representation space of mmWave signals with the text semantic space of large pre-trained language models through contrastive learning, thereby enabling the framework to leverage the generalizability of these language models for predicting unseen activities. However, accurate alignment of the two embedding spaces requires a substantial volume of paired signal-text data with diverse activity samples, and the paired real-world dataset is very limited. To address this, in our mmCLIP framework, we create a large synthetic dataset for pre-training and collect a small real-world dataset for fine-tuning our framework to bridge the sim-to-real gap. For fine-tuning, rather than directly adjusting the trained network parameters, we utilize the Low-rank Adaptation (LoRA [19]) framework, which allows for efficient model tuning on a very small parameter set. In addition, we design an activity attribute decomposition and recombination framework for both mmWave signals and text labels to characterize the relations among activities, facilitating the accurate classification of unseen activities. During the inference of an **unseen activity** label, for which our framework has never been trained on either the signal data or the exact text label of the corresponding activity, our mmCLIP model generates signal embedding for the unseen activity, identifies the closest matching text activity embedding from all candidate activities, and assigns the related label to the unseen activity. Correspondingly, the activities used in the fine-tuning process are regarded as **seen activities**.

### 2.1 Pretraining of mmCLIP

The objective of this step is to create a large paired signal-text human motion dataset to pre-train our proposed mmCLIP model, thereby enabling accurate alignment of the signal embedding space with the activity text space. This dataset is created by leveraging the existing online large human mesh dataset (i.e., BABEL [42]) with diverse human activities and corresponding language labels describing actions, and utilizing the signal simulator [58] to synthesize the corresponding mmWave signals from this dynamic mesh dataset by simulating the signal propagation and reflection on the mesh surface. In this way, we successfully build the synthetic dataset by pairing the simulated signals and the corresponding activity labels from the descriptive text.

Regarding the design of our mmCLIP model, as illustrated in Fig. 1, there are two branches (i.e., Text and Signal Branches). In the text branch, the activity text label in the synthetic dataset is fed into the Text Attributes Module. In this module, we first utilize the ChatGPT-based Attribute Describer to provide detailed descriptions of various attributes of the activity (e.g., a comprehensive description of the activity, how the subject’s arms or legs move during the activities, whether the subject changes location, etc.) using in-context learning [12]. Next, we feed the text attribute descriptions from ChatGPT into the CLIP-based Attribute Embedding Generator (i.e., a weight-frozen CLIP text encoder) to generate the text attribute embeddings for this text label. Subsequently, all the text

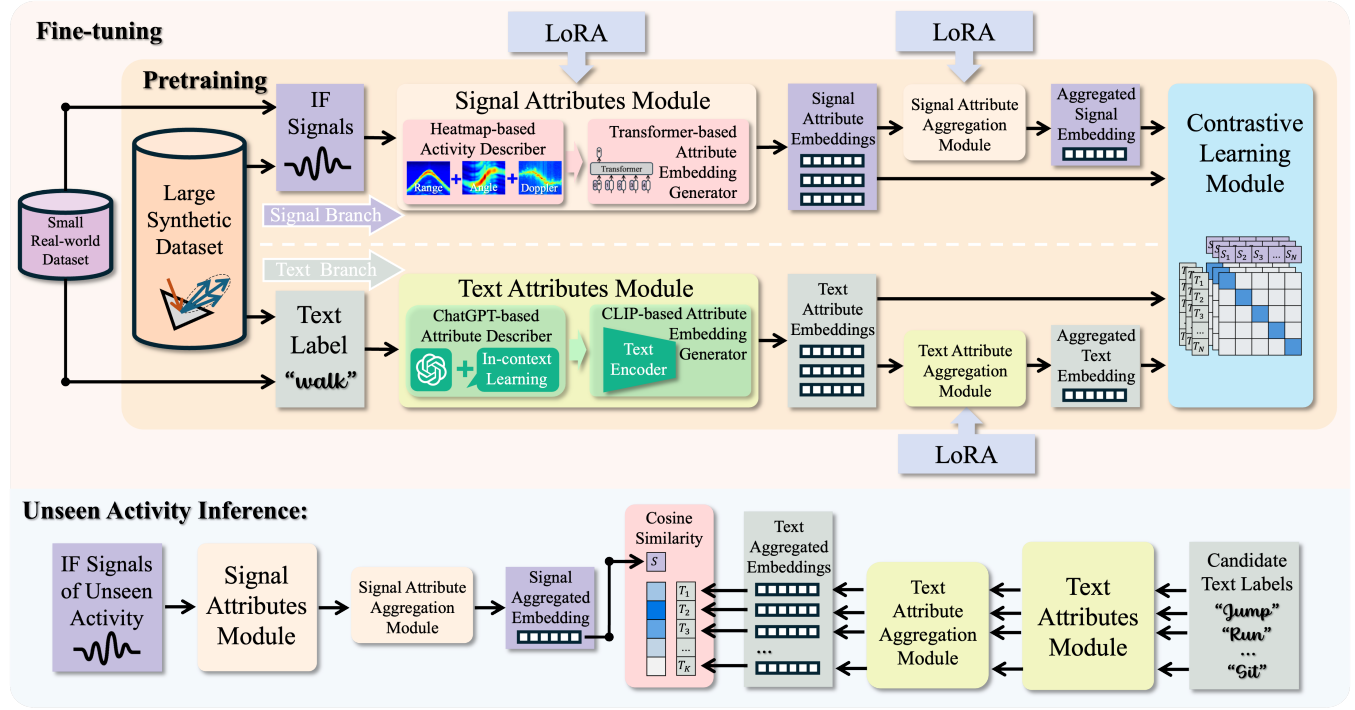


Figure 1: System Overview of mmCLIP Framework

attribute embeddings are fed into the Text Attributes Aggregation Module to obtain the aggregated text embedding that represents this text label before the contrastive learning step. In the signal branch of the model, the generated IF signals are fed into the Signal Attributes Module, which first generates three different heatmaps corresponding to the angle, Doppler, and range states of the activity. We then developed a hierarchical Transformer-based Attribute Embedding Generator to create attribute embeddings that correspond to the text attribute embeddings in the text branch. Similarly, all the signal embeddings are fed into the Signal Attributes Aggregation Module to obtain the aggregated signal embedding. Finally, we perform contrastive learning on the paired signal-text attribute embeddings and their corresponding aggregated embeddings within the Contrastive Learning Module. Specifically, this module focuses on pulling the signal embeddings toward the text embeddings that belong to the same activity, while pulling the signal embeddings against the text embeddings that belong to different activities in the embedding space. After the learning process, the signal embeddings are mapped to the text embeddings space, ensuring that signal and text embeddings related to the same activity are clustered together.

## 2.2 Fine-tuning of mmCLIP

To bridge the sim-to-real gap, we collect a small real-world dataset to fine-tune the mmCLIP model. Specifically, we employ the Low-rank Adaptation (LoRA), a model tuning framework, to fine-tune the parameters in the Signal Attributes Module and the Signal/Text Attributes Aggregation Module. This approach allows us to adjust the network parameters efficiently using only a small fraction of parameters, rather than retraining the entire model.

## 2.3 Label Inference of Unseen Activities

During the inference of unseen activities, we first feed the collected activity IF signals into the trained Signal Attributes Module and Signal Attributes Aggregation Module to generate the aggregated signal embeddings. Next, we input the candidate text labels into the Text Attributes Module and Text Attributes Aggregation Module to generate aggregated text embeddings for all the candidate text labels. To determine the class of the unseen pose, we find the closest matching text embedding from all candidate activities and assign the corresponding label to the unseen activity. By leveraging the descriptive capabilities of the ChatGPT model and the generalizability of the pre-trained CLIP model, our framework can generate embeddings for completely unseen labels, thus enabling unseen class classification.

## 3 METHODOLOGY

In this section, we will provide a detailed introduction to our proposed mmCLIP framework, which includes the model and training scheme designs.

In our model design, we design an activity attribute decomposition and recomposition approach to generate both the signal and text activity embeddings and employ the contrastive learning approach to align the signal with text embedding spaces. The rationale behind attribute decomposition and subsequent recomposition is to capture the subtle semantic relations among activities in the embedding space which enables our model to gain explicit clues and relations about the activities, thereby improving the recognition results for unseen activities. From the text perspective, although the

embeddings of all activity text labels in the CLIP embedding space are closely grouped due to contrastive learning with images, each activity is treated as an individual embedding. Consequently, the relationships among the activity text embeddings are not properly characterized. To address this, our model proposes to use in-context learning and ChatGPT to automatically decompose the activity text labels into activity attribute descriptions and further transform them into attribute embeddings using the CLIP text encoder. In this way, we can capture the semantic relations among activities, represented as the similarities of their attribute embeddings. From the signal perspective, contrastive learning forces the Signal Attribute Embedding Generator to produce signal attribute embeddings that are close to the corresponding text attribute descriptions, which compels the model to focus on patterns in the signals that are related to the corresponding activity attributes.

In the rest of this section, we illustrate how we decompose the activity inputs, both text and signals, into attributes using the Text Attribute Module (Sec. 3.1) and the Signal Attribute Module (Sec. 3.2), respectively. These attribute embeddings are then recomposed using the Text/Signal Attribute Aggregation Module (Sec. 3.3) into embeddings to represent the entire activity. Lastly, the contrastive learning is performed in the Contrastive Learning module (Sec. 3.4). For the training scheme design, we first pre-train (Sec. 3.5) our framework using the created synthesized dataset. Then, we collect a small real-world dataset to fine-tune (Sec. 3.6) our model. Lastly, we elaborate on how to conduct unseen activity recognition (Sec. 3.7).

### 3.1 Text Attributes Module

This module is designed to conduct attribute decomposition on activity text labels, thereby enabling the capture of subtle semantic relationships among activities in the embedding space. The decomposition process is accomplished in two steps. First, the activity text labels are decomposed into activity text attribute descriptions. This step is automated using the ChatGPT-based Attribute Descriptor, which leverages in-context learning by providing ChatGPT with template descriptions and task samples. Supported by the generative capabilities of ChatGPT, high-quality text attribute descriptions for any activity can be automatically generated. Second, the attribute descriptions are encoded into text attribute embeddings. This is achieved using the CLIP-based Attribute Embedding Generator, which utilizes CLIP's text encoder to transform text attribute descriptions into embedding representations.

**3.1.1 ChatGPT-based Attribute Descriptor.** In this design, we employ ChatGPT, a large language model (LLM) trained on extensive datasets of textual content, as our text attribute descriptor to facilitate the generation of high-quality motion descriptions for the activity text labels. While it may be feasible to manually decompose activity labels for tasks with a limited number of activities, as described later in Section 3.5, using a LLM like ChatGPT is essential for handling massive sets of text labels from the mesh dataset. To ensure the output aligns with our goal, we utilize in-context learning, an efficient method to enhance the performance of the LLM on specialized tasks. In-context learning does not require parameter fine-tuning; instead, it involves providing the model with task-specific descriptions and examples that help tailor its responses. As

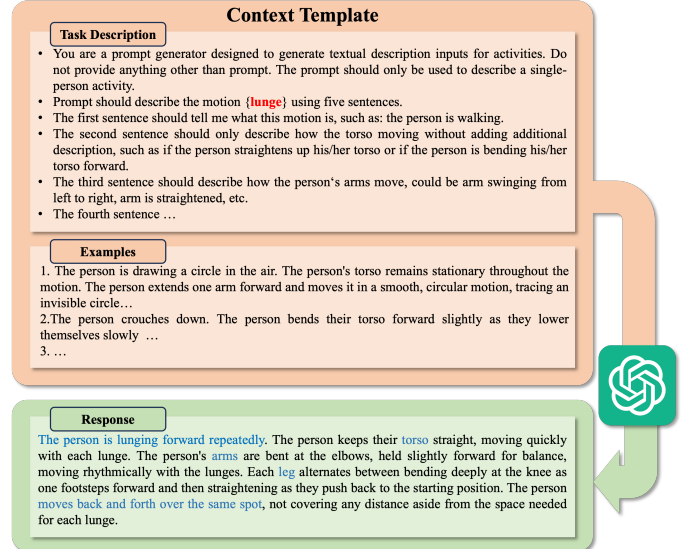


Figure 2: ChatGPT-based Attribute Descriptor

illustrated in Fig. 2, the LLM is provided with a context template, which includes a detailed task description and a few user-crafted examples (the user only needs to do this once for all the activities). The task description specifies the expected outputs of the activity text attributes, and the designed examples help ensure that the LLM's outputs align closely with our expectations. This ensures the LLM's output activity descriptions are accurate and relevant to the specific activity labels.

Specifically, for an activity text label  $y_i^T$ , we can decompose it into  $N$  text attribute descriptions  $\{T_n\}_{n=1}^N$ . In our design, the decomposed text attributes represent the different aspects of the activities and should also be sensible in the context of mmWave signals. Here are five attributes used in our paper. First, we include an augmented general description of the activity to preserve the comprehensive information encapsulated in the original activity label. Second, we decompose the activity based on body part movements, focusing on the torso, arm, and leg movements. These attributes are important since all the activities, whether seen or unseen, may share similar postures among certain body parts. By leveraging this design, the model can characterize the relationships among activities, which enables the use of semantic activity information to facilitate the recognition of unseen activities. Last, since the RF signal is sensitive to the target locational changes, we also incorporate an attribute description that explicitly details the locational changes occurring during the activity. As illustrated in Fig. 2, we prompted the ChatGPT to generate the text attribute descriptions of the activity “lunge”. By simply replacing the word marked in red with the designated activity, the ChatGPT model can automatically produce a satisfactory response that includes five sentences to describe the designed five attributes (marked in blue) accurately.

**3.1.2 CLIP-based Attribute Embedding Generator.** Contrastive Language-Image Pretraining (CLIP [43]) model is trained using contrastive learning on the image and text modalities. Trained on a large image and caption dataset, its text encoder can effectively capture the nuances and context of language, which is used as

the Attribute Embedding Generator to generate the attribute embeddings from the text descriptions. Specifically, after acquiring language attribute description  $\{T_n\}_{n=1}^N$  from ChatGPT-based Attribute Descriptor, we employ the CLIP text encoder to generate the attribute embedding  $\{t^n\}_{n=1}^N$ .

### 3.2 Signal Attributes Module

This module aims to generate signal attribute embeddings from the IF signals. To achieve this, we first utilize the designed Heatmap-based Activity Describer to generate the Time-Doppler (TD), Time-Range (TR), and Time-Angle (TA) heatmaps for the activity signals within a certain time window. Note that these heatmaps represent different aspects of the activities from the signal perspective, which is essential for recognizing complex activities, as ambiguous movement observed from a single heatmap may be more distinguishable when combining all of the attributes. For instance, solely using the TD heatmap may not sufficiently differentiate between clockwise and counter-clockwise walking. Adding the TA heatmaps helps resolve such ambiguities. Similarly, while the TR heatmap effectively distinguishes between stationary and mobile activities, it is less effective for detecting subtle micro-movements without changes in location. Then, we proposed the Transformer-based Attributes Embedding Generator to output the activity signal attribute embeddings to align with the text attribute embeddings in the previous section from the obtained heatmaps.

**3.2.1 Heatmap-based Activity Describer.** Given the collected IF signal data, we first perform a range Fast Fourier Transform along the axis of ADC samples and then remove static clutter by subtracting the mean value from each range bin. This process results in a radar data tensor of size  $\mathcal{R}^{N_p \times N_c \times N_r}$ , where  $N_p$  is the number of transceiver pairs,  $N_c$  is the number of chirps, and  $N_r$  is the number of range bins. To generate the TD, TA, and TR heatmaps, we begin by implementing a  $D$ -point sliding window with a step size of  $S$  along the chirp axis. This operation produces a sequence of windowed radar cubes, each of size  $\mathcal{R}^{N_p \times D \times N_r}$ . For the TR heatmap, we aggregate the values across the chirp and antenna axes for each windowed radar cube. This produces a sequence of vectors at different time points indicating the intensity of possible objects at each range bin. These vectors are then concatenated by the temporal order to form the final TR heatmap. Similarly, to generate the TA and TD heatmaps, we first perform an FFT along the antenna or chirp axis of each windowed radar cube, respectively. For the TA heatmap, we aggregate the values across the chirp and range axes, while for the TD heatmap, aggregation is performed across the range and antenna axes. Finally, we resize all the heatmaps to a uniform shape  $\mathcal{R}^{H \times T}$ , producing a 3-channel heatmap matrix  $M \in \mathcal{R}^{H \times T \times 3}$ .

**3.2.2 Transformer-based Attribute Embedding Generator.** In this section, we develop a transformer-based signal attribute embedding generator that hierarchically extracts features from the heatmaps and transforms them into detailed attribute embeddings. The process begins with three heatmap encoder branches, each dedicated to extracting radar features from one heatmap. Following this, an attribute token learner is employed to fuse and refine the attribute features obtained from each branch. The output from the attribute

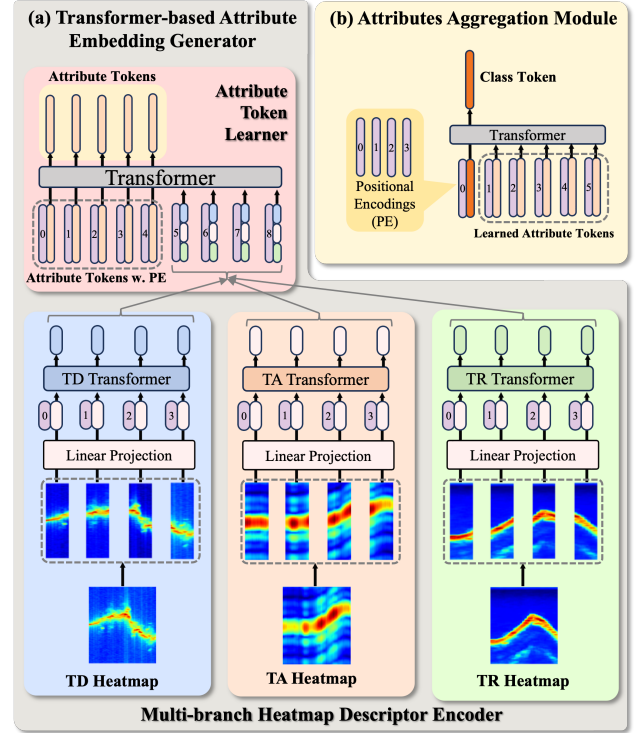


**Figure 3: Transformer-based Attribute Embedding Generator and Attributes Aggregation Module**

token learner is the attribute embedding, which will then be aligned with the text attribute embedding in the Contrastive Learning Module.

**Multi-branch Heatmap Descriptor Encoder.** As all the heatmaps have a time dimension, it is essential to efficiently model their temporal structure to extract useful motion features. In our design, we crop the heatmaps along the time dimension using sliding windows and feed the obtained patches into the encoder. This approach enforces the model to capture and analyze the changes along the temporal dimension. Specifically, given the input heatmap matrix  $M \in \mathcal{R}^{H \times T \times 3}$ , we first use three separate transformer encoders to extract heatmap features from each heatmap encoder. The encoding procedure includes three stages: patch embedding, temporal embedding, and self-attention. For the patch embedding, we apply a sliding window with size  $H \times w$  on the heatmap along the  $T$  axis to create a series of element time patches  $X \in \mathcal{R}^{\lfloor T/W \rfloor \times H \times w}$ . These patches will then be flattened and linearly projected into embedding  $X \in \mathcal{R}^{\lfloor T/W \rfloor \times D}$ . Such a design crops the heatmap as patches with sequential order, however, the temporal relationships among consecutive patches are not explicitly encoded. Because the self-attention operation is permutation invariant, the Transformer architecture itself does not have any information on the position of each patch. To this end, we add a pre-initialized learnable temporal embedding (i.e., positional encoding)  $P \in \mathcal{R}^{\lfloor T/W \rfloor \times D}$  to retain the absolute position information. In this way, we can obtain the position-encoded input element representation  $\hat{X} = X + P$ .

We then apply multi-head self-attention blocks to extract long-term interactions of features received at different patches for every

heatmap. Each self-attention head functions as an individual feature extraction layer that focuses on different positions in the heatmaps. Specifically, the temporal patches  $\hat{X} \in \mathcal{R}^{\lfloor T/W \rfloor \times D}$  is linearly transformed into the query  $Q$ , key  $K$ , and value  $V$  matrix with dimension  $\mathcal{R}^{\lfloor T/W \rfloor \times D/H}$ ,

$$Q = \hat{X}W_Q^T, K = \hat{X}W_K^T, V = \hat{X}W_V^T, \quad (1)$$

where  $W_Q, W_K, W_V$  are the linear transformation matrix and  $H$  is the number of heads. The attention function maps the query with the key-value pair and calculates the output with the weighted sum, which can be written as:

$$z_i = \text{Attention}(Q, K, V) = \text{softmax}\left(\frac{QK^T}{\sqrt{d_k}}\right)V \quad (2)$$

where  $d_k$  is the scaling factor. The output attention matrix  $z$  can be obtained by concatenating  $z_i$  from  $H$  attention head, and the final output for the encoder block can be written as  $z = \text{MLP}(\text{LN}(z)) + z$ , where  $\text{MLP}(\cdot)$  is a multi-layer perceptron and  $\text{LN}(\cdot)$  is layer normalization.

**Attribute Token Learner** Given the output  $\check{z} \in \mathcal{R}^{\lfloor T/W \rfloor \times D}$  from the transformer encoders of each branch, we concatenate the feature input along the embedding dimension  $\check{z} \in \mathcal{R}^{\lfloor T/W \rfloor \times 3D}$ . In this way, the attribute-specific features can be fused within the corresponding time window. In addition, we add  $N$  learnable token  $\{h^n\}_{n=1}^N$  of shape  $\mathcal{R}^{3D}$  as addition inputs to present the signal attributes embedding. Then, we obtain a concatenated embedding  $\hat{z} = [h^1; \dots; h^N; \check{z}]$ , which will be fed into a new transformer block to generate the signal attribute embeddings.

### 3.3 Attributes Aggregation Modules

From Sec. 3.1 and Sec. 3.2, we have obtained the text attribute embeddings  $\{t^n\}_{n=1}^N$  and signal attribute embeddings  $\{h^n\}_{n=1}^N$  of the activity. We employ the Signal/Text Attribute Aggregation Module to aggregate these signal/text attribute embeddings. While the structures of these two modules are identical, each module is trained with its own set of weights. As illustrated in Fig. 3 (b), we use a lightweight self-attention network to recompose the attribute embeddings into an aggregated embedding. Additionally, the model incorporates a learnable token (i.e.,  $t^{cls}$  in the text branch and  $h^{cls}$  in the signal branch) as an additional input embedding to represent the aggregated text/signal information for the activity. During the inference, these embeddings are utilized to calculate the similarity scores between the mmWave signal and candidate text labels.

### 3.4 Contrastive Learning Module

In this section, our goal is to train the entire framework that can generate meaningful signal attribute embeddings and properly combine the text and signal attribute embeddings. This is accomplished using contrastive learning which pulls positive pairs (e.g., signal and text embeddings belonging to the same activity) closer while pushes negative pairs (e.g., signal and text embeddings from different activities) further apart. Formally, for a batch of heatmaps, we first optimize the cosine similarity  $\text{sim}(\cdot)$  between text attribute embedding  $t^n$  and heatmap attribute embedding  $h^n$  via cross-entropy

loss

$$\mathcal{L}_{attr} = -\frac{1}{I} \sum_n \sum_i (\log \frac{\exp(\text{sim}(h_i^n, t_i^n)/\tau)}{\sum_j \exp(\text{sim}(h_i^n, t_j^n)/\tau)} + \log \frac{\exp(\text{sim}(h_i^n, t_i^n)/\tau)}{\sum_j \exp(\text{sim}(h_j^n, t_i^n)/\tau)}) \quad (3)$$

where  $i, j$  is the mini-batch index and  $\tau$  is the temperature parameter. We then compute the text class embedding  $t_i^{cls}$  and heatmap class embedding  $h_i^{cls}$  and optimize the class loss through cross-entropy:

$$\mathcal{L}_{cls} = -\frac{1}{I} \sum_i (\log \frac{\exp(\text{sim}(h_i^{cls}, t_i^{cls})/\tau)}{\sum_j \exp(\text{sim}(h_i^{cls}, t_j^{cls})/\tau)} + \log \frac{\exp(\text{sim}(h_i^{cls}, t_i^{cls})/\tau)}{\sum_j \exp(\text{sim}(h_j^{cls}, t_i^{cls})/\tau)}) \quad (4)$$

The final loss is calculated by combining the attribute and class loss as follows:

$$\mathcal{L}_F = \lambda_\alpha \mathcal{L}_{attr} + \lambda_\beta \mathcal{L}_{cls} \quad (5)$$

where  $\lambda_\alpha$  and  $\lambda_\beta$  are the hyper-parameters.

### 3.5 Model Pretraining using Large Synthetic Dataset

In this paper, our objective is to achieve zero-shot human activity recognition on the mmWave-based sensing system. To accomplish this, we propose to take advantage of the generalizability of the Visual Language Models (VLM). A critical component of this approach is the development of a large signal-text human activity dataset with diverse human activities, which will enable accurate alignment between the signal and text embedding spaces. However, collecting mmWave sensing data is uniquely challenging due to the need for specialized hardware and software, significant participant involvement, and meticulous environment preparation. These requirements make large-scale data collection both costly and logistically complex. To address this problem, we propose to leverage the abundant human mesh data in computer vision to generate a large synthesized dataset and pre-train our framework using the synthesized dataset. In computer vision, we can directly obtain the 3D mesh data of human motion from the abundant 3D human mesh datasets [33] or apply mesh estimation algorithms [15] on the large activity motion video datasets [26]. Existing work [58] has demonstrated that the IF signals can be directly simulated from the 3D human mesh which demonstrated effectiveness on challenging pose estimation tasks. In this way, we can obtain a large synthetic dataset with paired text labels and mmWave signals.

**IF Signal Simulation** In computer graphics, the human mesh is a three-dimensional model that represents the human body with a collection of triangle faces that define the shape of the body in the virtual space. For a human pose consisting of a set of triangular faces at time  $\{F_i^t\}_{i=1}^I$ , the first step is to identify the visible triangular faces from the perspective of the transceiver at locations  $L_T$  and  $L_R$  in  $\mathcal{R}^3$  using the Hidden Point Removal (HPR) algorithm [25]. To simulate the IF signal, it is necessary to determine the phase and strength of the reflected signal at each time  $t$  for each triangular face  $F_m^t \in \mathcal{R}^3$ . We denote the center locations, surface norms, and

areas of all visible triangular faces at time  $t$  as  $\{F_m^t\}_{m=1}^M$ ,  $\{N_m^t\}_{m=1}^M$ , and  $\{A_m^t\}_{m=1}^M$ , respectively.

The phase of the mixed IF signal for each triangular face at time  $t$  is calculated as  $p(t) = \exp(j2\pi(f_0\tau_m^t + St\tau_m^t))$ , where  $f_0$  is the starting frequency of the chirp signal,  $S$  is the frequency slope,  $\tau_m^t = (||L_T - F_m^t|| + ||F_m^t - L_R||)/c$  is the time-of-flight of the chirp signal received after reflected from the triangular faces,  $c$  is the speed of light, and  $||\cdot||$  is the Euclidean distance. To calculate signal strength, factors such as the angle of the mesh triangles to the transceivers, the distance from the mesh triangles to the transceivers, and the size of the mesh triangles are considered. We use the quasi-specular reflector model [28], which calculates the reflection ratio of a triangular face  $F_m^t$  by  $C_m^t = \exp\left(-\frac{\theta_t^2}{2\sigma^2}\right)$ , where  $\sigma$  is an empirical parameter and  $\theta_t$  is the angle between the strongest reflection direction and the received signal direction, calculated using the face norm  $N_m^t$ .

The simulated IF signal at time  $t$  is obtained by summing up the IF signals from each of the visible triangular faces:

$$s(t) = \sum_{m=1}^M \frac{A_m^t C_m^t p(t)}{||L_T - F_m^t|| \cdot ||F_m^t - L_R||} \quad (6)$$

For each transceiver pair, we apply the same process and sum up the IF signals. Finally, we introduce Gaussian white noise to the aggregated IF signal to simulate the thermal noise in real-world electrical circuits.

### 3.6 Real-world Data Fine-tuning

We incorporate an additional local fine-tuning step to bridge the sim-to-real gap using a small amount of real-world data. For the fine-tuning process, we employ Low-rank decomposition (LoRA) [19], a method that trains only a small fraction of parameters instead of training the entire model parameters. Specifically, for a pretrained weight matrix  $W \in \mathcal{R}^{m \times n}$ , LoRA constrains the update  $\Delta W$  through a low-rank decomposition  $W + \Delta W = W + BA$ , where  $B \in \mathcal{R}^{m \times r}$ ,  $A \in \mathcal{R}^{r \times n}$ , and the rank  $r \ll \min(m, n)$ . During training,  $W$  is frozen and does not receive gradient updates, while  $A$  and  $B$  contain trainable parameters.

**Fine-tuning Loss Function.** Since the number of training samples in each batch may exceed the number of distinct activity labels in the training data for fine-tuning, multiple training samples corresponding to the same activity label can appear in a training batch. As a result, there can be more than one positive pair in a batch. Therefore, treating the similarity score learning as a simple 1-in-N classification problem with cross-entropy loss is inappropriate [54]. Instead, we employ the Kullback–Leibler (KL) divergence as the signal-text contrastive loss to optimize our framework, enhancing the model's ability to distinguish between the positive and negative pairs effectively. Specifically, let  $p(h, t)$  and  $q(h, t)$  represent the ground truth and estimated similarity matrices for each batch, respectively. Correspondingly, we derive the symmetric matrices  $p(t, h)$  and  $q(t, h)$ . The loss function can be re-written as:

$$\mathcal{L}_{cls} = \frac{1}{2} \mathbb{E}_{(h,t) \in D} (KL(p(h, t), q(h, t)) + KL(p(t, h), q(t, h))) \quad (7)$$

where  $D$  is the entire dataset.

### 3.7 Zero-shot Inference

For all the unseen activity text labels, we can apply the Text Attributes Module and the Text Attribute Aggregation Module to generate the aggregated text embedding  $t^{cls}$ . Similarly, we can encode the radar signal using our Signal Attribute Module and the Signal Attribute Aggregation Module to generate the aggregated signal embedding  $h^{cls} \in \mathcal{R}^D$ . The recognition task is then reformulated to

$$\hat{y} = \arg \max_{y_i \in Y} \frac{\exp(\text{sim}(h^{cls}, t_i^{cls})/\tau)}{\sum_{i=1}^C \exp(\text{sim}(h^{cls}, t_i^{cls})/\tau)} \quad (8)$$

By modeling the recognition process as calculating the similarity between radar signal embedding and text embeddings, the model can recognize new activities.

## 4 SYSTEM IMPLEMENTATION

### 4.1 Testbeds

As illustrated in Fig. 4 (a), (b), we employ the TI AWR1843 BOOST mmWave radar [52], coupled with the TI DCA1000 evaluation module, to collect and stream mmWave data. The radar system comprises three transmitting and four receiving antennas, which emit and receive Frequency Modulated Continuous Wave (FMCW) signals. Each FMCW chirp spans a bandwidth of 3.9 GHz, increasing linearly from 77 GHz to 80.9 GHz. The radar is configured to transmit 10 frames per second, synchronizing with the frame rate of online mesh data. Each frame consists of 128 chirps, with each chirp containing 256 sampling points. Given these device settings, our mmWave setup can achieve a sensing range of up to 11 meters, a range resolution of 4.3 cm, a sensing velocity of 4.5 m/s, and a velocity resolution of 7.1 cm/s. In our experimental setup, the mmWave testbed is placed on a table at a height of around 1 meter, with the distance between the radar and the subject varying from 1 to 6 meters. Additionally, four Zed 2i stereo cameras [49] are deployed and fused to capture high-quality skeletal data for each activity simultaneously. These skeletal structures are then utilized to generate the SMPL parameters using SMPLify [3].

### 4.2 Synthetic Data Preparation

We utilize the AMASS [33] human motion capture dataset, complemented by paired textual labels from the BABEL [42] and HumanML3D [18] datasets, as our source for synthetic data. AMASS is an extensive motion capture corpus featuring over 50 hours of continuous motion sequences, which encompass more than 200 daily activity classes performed by 500 subjects. The Babel dataset provides frame-level short and general textual descriptions for these motion sequences. For our purposes, we first generate a textual label for each sequence by listing all actions within a specific action window, then concatenating them into a single string. This concatenated string is then fed into the text attribute module for attribute generation. The HumanML3D dataset provides an additional source of textual labels for the AMASS dataset, offering four general textual descriptions written by different human labelers for each continuous motion sequence. Given that our activity observation window lasts only 3 seconds, we selectively use motion sequences that are shorter than 5 seconds to ensure that the textual labels

are accurately aligned with the motion sequences. Similarly, the original textual label from HumanML3D will be parsed by our text attribute module for attribute generation. Note that although the textual labels from BABEL and HumanML3D provide descriptions, they are generally broad and pertain to specific motions. These descriptions lack the detailed granularity necessary for limb motions, thus posing a challenge for the model to accurately capture subtle activity relationships without the motion decomposition module.

The radar is positioned three meters in front of the subject and mounted at a height of 1 meter above the ground at the start of each motion sequence. The designated activity area for the subject is confined to a 5m by 6m space, accommodating a wide range of daily activities. We employ the same chirp configuration in our signal simulation as we use for collecting real local mmWave data, ensuring consistency between synthetic and real-world datasets. By combining all of the motion sequences and labels from these datasets, we obtained a diverse synthetic RF dataset comprising 30 hours of high-quality paired synthetic text-radar samples.

### 4.3 Model Training Detail

We employ the CLIP-ViT-B-32 as the pretrained model for our CLIP-based text embedding generation module. For textual attribute generation, we set the number of attributes as 5 and utilize GPT4-turbo for label generation. For the multi-attribute heatmap generator, we utilize a window of 256 chirps with a 16-chirp interval. In our transformer-based attribute embedding generator, we employ a 2-layer transformer block for initial extraction in each branch, followed by a 6-layer transformer block with 8 attention heads in the property learner module. In the attribute aggregation module, we utilize a lightweight single-layer transformer block. We optimize our models using the Adam optimizer with a learning rate of 0.0001 and apply exponential weight decay at a rate of 0.9 after each epoch. As stated in Equation 5, the hyperparameters  $\lambda_\alpha$  and  $\lambda_\beta$  are set to 1. All deep learning models are implemented using PyTorch [40] and trained on NVIDIA A100 GPUs.

## 5 EXPERIMENTS

### 5.1 Experiment Setup

**5.1.1 Local Data collection.** In our experiment, we design and collect radar data including a total of 60 activities across three different environments<sup>1</sup> that cover common activities in real-world scenarios to evaluate our system, as illustrated in Fig. 4 (a), (c), (d). These activities can be divided mainly into three categories: fitness activities (e.g., squats, jumping jacks, lunges, etc.), daily activities (e.g., drinking water, walking in a circle, sitting, etc.), and gesture controls (e.g., drawing a circle, swiping left, etc.), ensuring diversity in the activities. We recruited 8 subjects with heights ranging from 165 cm to 185 cm to perform these activities repeatedly for duration between 30 and 60 seconds in front of the mmWave radar. This contributes a dataset with approximately 6 hours of real-world sensing data. During these sessions, we simultaneously collected the IF signal data from the mmWave radar and corresponding pose data from four stereo cameras. It is important to note that the pose data generated from the stereo cameras is not used in the synthetic data

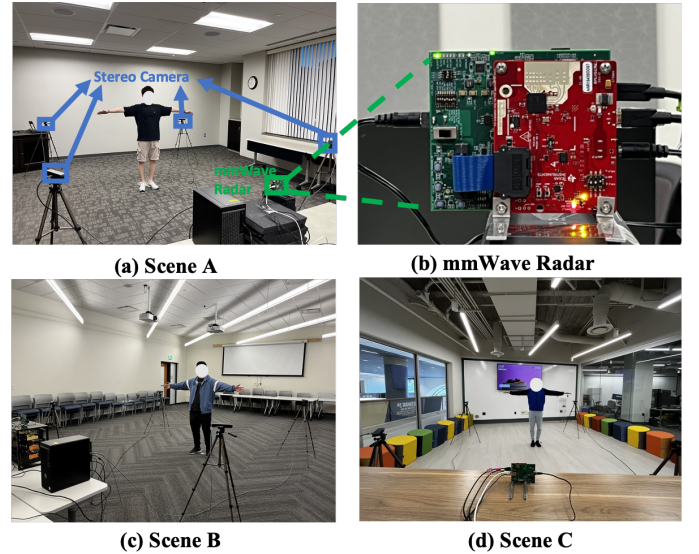


Figure 4: Experiment Setup

pretraining and is only utilized in Sec. 5.5 to evaluate the quality of our simulator. Most activity cycles are less than 3 seconds, aligning with our radar signal observation window, except for mobile activities such as walking in a circle, and walking forward and backward which take more time to finish an activity cycle. In the default setting, we use three non-overlapping 10 classes as the unseen class groups. For each group, we use the rest of 50 classes as the seen activities. We repeat the experiment 3 times for each group and then calculate the final result by averaging the result from each group. In the scenario with fewer than 50 seen classes, we maintain the same group of unseen activities. To adjust the number of seen activities, we randomly remove excess activities from the seen activity group. This procedure is repeated three times to ensure variability and robustness in our results.

**5.1.2 Models for Evaluation.** In our experiments, we mainly evaluate the text attribute module, synthetic dataset pertaining module, and real data fine-tuning module with the model setting as follows:

**Tent:** Tent [64] is a pioneering work designed for zero-shot human activity recognition by aligning multiple sensing modalities, including mmWave, LiDAR, and video, with CLIP's text embedding space. The model proposed in Tent receives mmWave radar point cloud as input and utilizes a limited set of real-world mmWave point cloud data from seen activities for model training. It further adopts a learnable soft prompt [63] to enhance the understanding of textual information. For a fair comparison, we modified Tent's input modality to heatmap and adjusted the corresponding network structure accordingly.

**Real:** This baseline model configuration is the minimum implementation of our model, which utilizes only a set of real-world data from seen activities for model training, without integrating the text attributes module and synthetic dataset, sharing the same design principle as Tent [64].

**Syn:** In this basic model setting, only the large synthetic dataset is used for model pretraining, without incorporating real data fine-tuning or the text attributes module.

<sup>1</sup>All the data collection was approved by the IRB of the authors' institution.

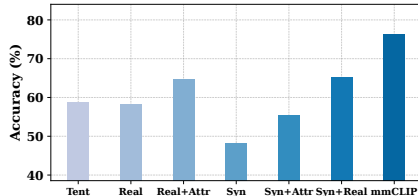


Figure 5: Overall Zero-shot Performance

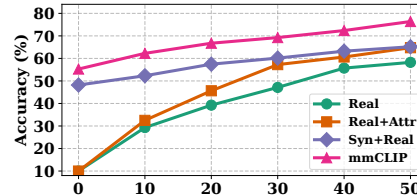


Figure 6: Effect of Seen Activities

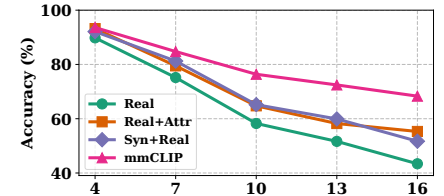


Figure 7: Effect of Unseen Activities

**Real+Attr:** This model employs real data from the seen activities along with the text attributes decomposition module without utilizing the synthetic dataset for pretraining.

**Syn+Attr:** This baseline model is enhanced with the synthetic dataset pertaining and our proposed text attribute decomposition module, but it does not include fine-tuning with real data from seen activities.

**Syn+Real:** This model combines synthetic dataset pretraining with real data fine-tuning but does not incorporate the text attribute decomposition module.

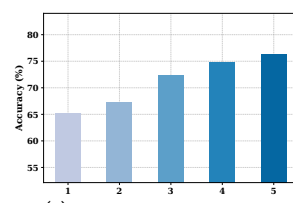
**mmCLIP:** This is the full implementation of our proposed model, incorporating synthetic data pretraining, real data fine-tuning, and the text attribute decomposition module.

## 5.2 Overall Zero-shot Performance

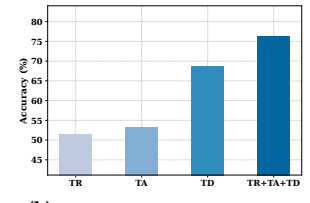
In this section, we evaluate the overall zero-shot performance of the mmCLIP model and compare it with multiple baseline methods introduced in Sec. 5.1.2. As demonstrated in Fig. 5, our proposed mmCLIP model achieves superior performance in classification accuracy compared to all of the baseline methods, with a notable 76.4% average classification accuracy on three non-overlapping 10-class unseen activity groups. Note that in our zero-shot setting, the model can not access the data from unseen activities during training, which brings a significant challenge to the classification task. We can see that the performance of the Real baseline closely mirrors that of Tent; however, both fail to produce satisfactory results due to the absence of synthetic data pre-training and the attribute decomposition module. It can also be seen that the performance of models Real+Attr, Syn+Attr, and mmCLIP decreases significantly when the attribute decomposition module is removed. This underscores the effectiveness of our proposed attribute decomposition module, which characterizes subtle relations among activities to facilitate zero-shot inference. Additionally, we can see the performance of Syn+Real exceeds that of Syn by a large margin, which is trained only on the synthetic dataset. The unsatisfactory performance from model Syn is due to the existence of a simulation-to-reality gap between the synthetic dataset and real-world radar signals, demonstrating the effectiveness of our fine-tuning approach in mitigating this gap, thereby enhancing zero-shot activity recognition performance.

## 5.3 Study of Zero-shot Settings

**5.3.1 Effect of Number of Seen Activities.** In this section, we investigate the impact of the number of seen activities on zero-shot performance. As illustrated in Fig. 6, an increase in the number of seen activities from 0 to 50 classes significantly enhances the model's performance, with optimal results observed at 50 classes. We can



(a) Effect of Text Attribute



(b) Effect of Heatmap Attribute

Figure 8: Effect of Attribute Decomposition

see mmCLIP consistently outperforms other baselines (without text attribute module or synthetic data pertaining) across varying class sizes, demonstrating the effectiveness of our proposed attribute decomposition module and synthetic data pretraining. It is noteworthy that mmCLIP with 0 seen activity (without fine-tuning) achieves comparable results to the model Real+Attr with 30 seen classes. This outcome highlights the advantage of synthetic data pretraining, which leverages large-scale synthetic datasets to reduce data collection efforts while maintaining decent performance.

**5.3.2 Effect of Number of Unseen Activities.** We also explore the impact of the number of unseen activities on mmCLIP's scalability in real-world deployments. In Fig. 7, we show the model's performance as the number of unseen classes increases from 4 to 16 with an interval of 3. Initially, all models exhibit decent performance for simpler classification tasks (e.g., 4 classes). However, as the classification task becomes more challenging (e.g., 16 classes), the performance of baseline models significantly decreases. In contrast, mmCLIP maintains robust performance despite the increase in classification complexity (e.g. above 68% in 16-classes classification). This demonstrates our proposed attribute decomposition module and synthetic data pretraining strategy can transfer effective knowledge from pervasive text and visual data and characterize the nuanced relationship between activities.

**5.3.3 Effect of Attribute Module.** In this section, we evaluate the impact of our text and heatmap attribute modules on model performance, as illustrated in Fig. 8. For the text attributes module, we assess the performance impact by varying the number of attributes from 1 to 5. In Fig. 8a, the results show that the model performance improves consistently with the increase in the number of attributes. This result supports that more attributes allow for a more distinctive characterization of activities, enabling our model to use these attributes as effective cues to infer unseen activities.

For the heatmap attribute decomposition module, we choose three baseline models by retaining only one attribute. As shown in Fig. 8b, the performance of TD heatmap is better than TR and TA. This is possibly because the Doppler attribute is more sensitive to subtle body part movement compared to the range and

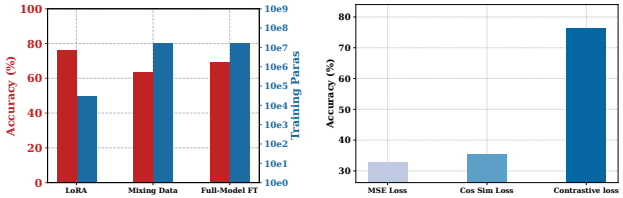


Figure 9: Effect of Fine-tuning

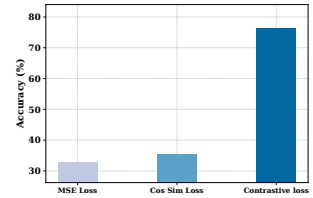


Figure 10: Effect of Loss Function

angle attributes, thus enabling more distinguishable motion features for classification. However, none of these baseline approaches surpassed mmCLIP, which underscores that integrating multiple attributes allows our heatmap encoder to learn detailed activity features that align with text attributes to infer unseen activities more effectively.

**5.3.4 Effect of Fine-tuning Methods.** In this section, we assess the accuracy and fine-tuning overhead of LoRA in our model by comparing it with different baseline fine-tuning methods. In addition to LoRA, we explore two additional fine-tuning baselines: (a) mixing data from the synthetic dataset with data from the real-world activity dataset and training the model from scratch, and (b) full-model fine-tuning with the pretrained model from the synthetic dataset. As shown in Fig. 9, we observe that fine-tuning approach (a) is not effective in both classification accuracy and training overhead. The reason behind this is that this approach needs to train the full model and the training process is dominated by the overwhelming volume of synthetic dataset, thus leading to unsatisfied performance. Approach (b) also shows suboptimal results due to the requirement of adjusting all model parameters, which often leads to the issue of catastrophic forgetting. Our model, on the other hand, archives the best classification accuracy with only utilizing 0.25% training parameter compared to the baseline methods, demonstrating the effectiveness of our fine-tuning method.

**5.3.5 Effect of Loss Function.** In this section, we evaluate the impact of different loss functions on model performance. We examine two commonly used loss functions as our baseline: (a) cosine similarity loss, and (b) mean-square error (MSE) loss. For these baseline loss functions, we compute the loss only for each positive sample (paired heatmap data sample and text sample) without explicitly distinguishing the negative samples (unpaired heatmap data sample and text sample). The results, as shown in Fig. 10, indicate that neither baseline loss function can show satisfied performance in the zero-shot classification task. The reason is that the baseline loss functions focus solely on making the embeddings of the same class similar, while the contrastive losses not only account for the intra-class alignment of embeddings but also consider the interconnection between different classes. This result demonstrates that our contrastive loss function is more effective in creating a robust semantic space for each activity, as it enhances both intra-class alignment and inter-class differentiation.

**5.3.6 Cross-Environment Zero-shot Performance.** We now evaluate the generalization ability of our system to different environments. We use Scene A (a conference room) as our basic environment, and use Scene B (another conference room), and Scene C (a resting area) as the test environment. Specifically, we pre-train the model with the synthetic dataset, which is environment-independent, then we

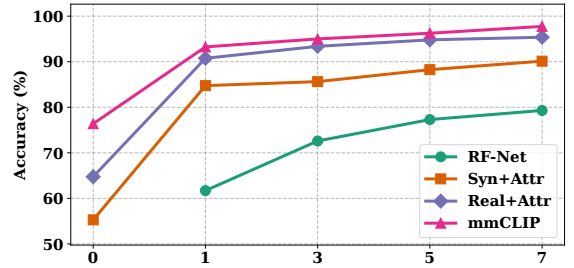


Figure 11: Few-shot Performance

fine-tune the model with the real seen activity data from the base environment and test it in the other environments with the same set of subjects. During the experiment, the subjects are asked to perform the same activities as they did in the base environment. The classification results for Scene A (base environment), Scene B (test environment), and Scene C (test environment) are 76.4%, 72.4%, and 75.3%, respectively. We can see only a marginal performance drop when transitioning from the base to the test environments. This robustness can be attributed to our synthetic data pre-training strategy, which enables the model to learn motion-specific features independent of the environment, thus enhancing its ability to generalize across different scenarios.

#### 5.4 Few-shot Performance

While zero-shot recognition is highly promising for training generalizable models capable of handling unseen classes, a few labeled samples from unseen activities may be available in practical scenarios to boost the model's performance. This motivates us to also evaluate our framework in the few-shot setting. A typical few-shot learning scheme [14, 27, 39] works by first pretraining a model on a set of base classes with sufficient labeled data to learn general features and representations. After this pretraining phase, the model is fine-tuned to quickly adapt and recognize new classes using only a small number of labeled examples from those classes, leveraging techniques like meta-learning or transfer learning to efficiently generalize to new tasks with limited data. These approaches struggle to work in zero-shot scenarios, which distinguishes our method from the approaches tailored exclusively for few-shot learning. In our approach, the synthetic data pre-training and real data fine-tuning of seen activities enable our model to capture effective feature representations from various activities. This foundation allows our framework to be easily extended to few-shot learning scenarios.

We employ a basic metric-based few-shot method that requires no additional training. Specifically, using a few representative heatmap examples from each unseen class, we can calculate the corresponding heatmap class embeddings. During the inference stage, we compute the heatmap class embedding from incoming heatmap samples and assess the similarity with the few-shot heatmap class embedding. The class label is then determined by selecting the class with the highest similarity. To compare with the existing few-shot framework, we have adapted RF-Net [11] as the few-shot baseline. Specifically, we adapted the selection of meta-tasks chosen from different environments for the same activity, to now be selected from among the base classes, followed by fine-tuning for the target classes.

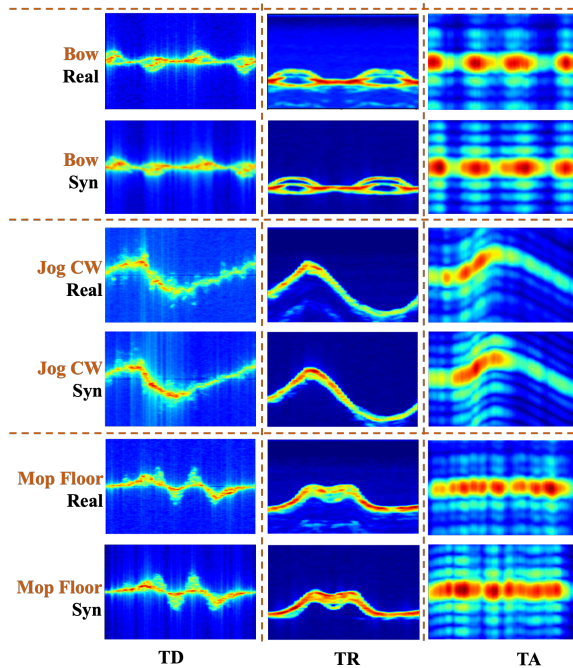


**Figure 12: Synthetic Heatmap Visualization**

As illustrated in Fig. 11, there is a clear increasing trend in classification accuracy for all models as the number of few-shot examples increases from zero-shot to 7-shot settings. With just a one-shot sample provided from each unseen class, our model achieves significantly higher accuracy compared to the zero-shot setting. This improvement is mainly because the model in the zero-shot setting relies solely on the semantic connection between activities to infer unseen classes while the model in the few-shot setting can leverage the representative samples from unseen activities as an observation to approximate the real distribution of unseen classes to enhance prediction. We also observe that our approach consistently outperforms the RF-Net baseline, this is because RF-Net is tailored primarily for adapting the same activity across different environments, thus it may not be able to efficiently handle the few-shot learning scenarios studied in this paper, whose goal is to recognize new activities with only a few labeled samples. Additionally, our framework leverages the powerful representation capabilities of the large pre-trained model, thereby helping to construct a robust feature space even with a limited dataset. It is also noteworthy that the model Syn, which is pre-trained on the synthetic dataset, achieves decent performance in the one-shot setting. This highlights the effectiveness of the synthetic data pre-training strategy that helps the model capture useful activity motion features with diverse activity motion data from other modalities at minimum data collection effort.

## 5.5 Quality of The Signal Simulator

In this section, we evaluate the quality of our signal simulator, which shares the same design principle as [6, 61]. Specifically, we first utilize the collected activity pose data to simulate radar signals for all 60 activities. We then train the model in the same manner as we pre-train mmCLIP using the large synthetic dataset and subsequently

test it on various unseen classification tasks using real-world radar signals. In this setting, our model achieves an impressive accuracy of 89.7%, demonstrating the simulator's capability to capture essential motion features beneficial for our zero-shot classification task, although it may not perfectly replicate the physical world. In Fig. 12, we show an example heatmap attribute from the activity bowing, jogging clockwise, and mopping the floor. The odd rows display the real heatmap signals captured during the activity, while the even rows illustrate the synthetic heatmap signals generated by our simulation module. The columns from left to right correspond to time-Doppler, time-range, and time-angle heatmaps, respectively. The visual similarity between the real and simulated signals underscores the effectiveness of our signal simulation module.

## 5.6 System Complexity and Latency

In this section, we analyze the computational complexity and the latency of the proposed system. For the complexity of our proposed mmCLIP framework, we report the number of trainable parameters in the deep learning model. In the synthetic data pertaining stage, the overall number of trainable parameters is  $20M$ , where the text branch has  $4M$  parameters and the signal branch has  $16M$  parameters. Compared with the original CLIP model with a total  $150M$  parameters [62], we can see our model is substantially more compact, enhancing its efficiency for the Human Activity Recognition task. During the fine-tuning stage, the total number of trainable parameters is reduced to  $500K$ , with the text branch accounting for  $30K$  parameters and the signal branch for  $470K$  parameters. This reduction highlights the efficiency of LoRA fine-tuning. For latency measurements, we conducted inference on a desktop equipped with an NVIDIA A6000 GPU and an Intel Xeon Gold 6254 CPU, reporting the average latency. Given that the text embedding can be computed in advance of the inference stage, the primary latency originates from the signal branch, which has a processing time of approximately  $7ms$ . This performance demonstrates that our proposed system is capable of operating in real-time, making it suitable for real-world applications.

## 6 RELATED WORK

### 6.1 mmWave-based Human Activity Recognition

The advancements in deep learning have spurred the development of various mmWave-based sensing systems for human activity recognition [5, 23, 29, 48, 59]. These systems employ various signal processing techniques to manipulate signal attributes into formats suitable for neural networks. However, a common limitation of these approaches is their dependence on abundant training data to achieve optimal performance. This requirement can pose challenges in real-world applications where such extensive data collection may not be feasible.

### 6.2 RF-based Zero-shot Human Activity Recognition

Due to the substantial effort required to collect mmWave signal datasets, recent research has explored few-shot and zero-shot activity recognition to improve the model's generalizability with limited

or no data. Studies such as [11, 16, 57] have proposed few-shot learning systems where the model is pretrained on a source dataset and benefits from a few representative samples in unseen classes to enhance its generalizability. In the zero-shot setting, where real-world signal data from unseen classes is not accessible, the classification challenge significantly increases. To address this, researchers have developed two primary approaches for zero-shot recognition using RF signals: the signal simulation-based approach and the semantic space projection-based approach. For the signal simulation-based approach, works like [1, 9] proposed simulating the initial Doppler heatmap from vision data of the unseen activity and refining it through deep neural networks. [6, 61] developed more sophisticated simulators capable of generating high-quality IF signals from vision data. To achieve zero-shot recognition, these works require the unseen activity label available in the training stage to synthesize radar signals using the physical simulator. These synthesized signals are then used to train a classification model with fixed output classes tailored to these predetermined classes to achieve zero-shot recognition. Such a design inherently limits flexibility, as the trained classification model would fail in scenarios where new unseen activities are encountered. In contrast, this paper addresses a more practical yet challenging problem, where both the signal and the label of the unseen activities are not observed during model training. To tackle this problem, our approach leverages language reasoning, utilizing pre-trained text embeddings and their semantic relationships to bridge the gap between seen and unseen classes. This enables our model to train on a set of seen activities and generalize to different unseen activity classification tasks, without explicitly acquiring unseen activity labels in the training stage.

On the other hand, the semantic space projection-based approach involves projecting the signal embedding space to the embedding space of other modalities that have been trained on a larger dataset to enhance zero-shot capabilities. For example, [21] utilized text semantic space with word embedding to bridge unseen and seen activities. Most recently, [64] proposed incorporating a text encoder from an existing visual-language model, such as CLIP [43], to facilitate the zero-shot recognition task. Unlike these approaches, our mmCLIP framework employs a pre-train & fine-tune training scheme that utilizes cross-modal signal synthesis to augment diverse mmWave data for pre-training, coupled with small real-world datasets for fine-tuning, to enhance the alignment of embedding spaces between radar signals and textual labels. Additionally, we designed an attribute decomposition and recombination module for both the signal and text modality. This helps the model to characterize subtle activity relationships leveraging the element activity attribute that may be shared between seen and unseen activities, thereby substantially improving classification performance for unseen classes.

### 6.3 Visual Language Models

Foundational visual language models (VLMs), such as CLIP [43] and ALIGN [22], have been extensively trained via contrastive pre-training using large-scale image-text pairs, demonstrating remarkable zero-shot transfer capabilities across a variety of downstream vision tasks. These applications include few-shot and zero-shot image recognition [60, 62, 63], object detection [17, 53, 56], image captioning [7, 34], cross-modal retrieval [13, 32], and video-based

HAR [30, 36, 46]. However, adapting pre-trained visual language models to radar-based HAR introduces significant challenges due to the absence of temporal information in image-based training data and the modality gap between image-text and signal-text pairs, necessitating innovative approaches to bridge these gaps.

## 7 DISCUSSION AND FUTURE WORK

While mmCLIP represents a pioneering endeavor towards a more generalizable Human Activity Recognition (HAR) system by leveraging knowledge from a pre-trained visual-language model, it opens up substantial avenues for future research:

**Different Radar View and Subject Position:** mmCLIP is primarily evaluated under conditions where the subject maintains a forward-facing orientation relative to the radar while engaging in most of the activities. In practical settings, variations in the radar's view direction and the subject's orientation can significantly alter the reflection patterns. This variability poses substantial challenges to the zero-shot recognition of unseen activities, underscoring the need for further development to accommodate a range of orientations and positions. A promising direction for future research includes simulating signals by adjusting the radar view and subject location to better mimic real-world scenarios.

**Multi-Modal Sensing:** A critical future direction for mmCLIP involves enhancing its capabilities to support multi-modal sensing. By delving into attribute decomposition, mmCLIP combines the physical signals with textual attributes. This methodology facilitates integration with other sensing modalities that utilize different physical properties, thereby enhancing environment perception for a more robust analysis.

**Adapting To Different Downstream Tasks:** Broadening mmCLIP's utility to encompass various downstream tasks such as virtual reality interactions, elderly care, and gesture recognition presents another promising avenue. This expansion could be facilitated by developing a larger vision-text dataset that captures diverse human motions across different contexts, utilizing 3D mesh generation tools [15] for synthetic dataset generation.

## 8 CONCLUSION

In this paper, we tackle the problem of mmWave-based zero-shot human activity recognition. Specifically, we propose mmCLIP, a novel mmWave sensing system that can recognize unseen activities by transferring knowledge from the advanced pretrained visual language model, which is pre-trained through pervasive text-image pairs. To facilitate the knowledge transfer process, we generate a comprehensive synthetic mmWave radar dataset by leveraging existing cross-modal vision datasets. Additionally, we introduce an attribute decomposition module that effectively characterizes the nuanced relationships between activities. Such model design enhances our system's ability to understand and classify complex activity patterns. The superior zero-shot classification results on unseen activities demonstrate the effectiveness of our proposed mmCLIP framework.

## 9 ACKNOWLEDGEMENT

This work was supported in part by the US National Science Foundation under Grants CNS-2154059 and IIS-2348427.

## REFERENCES

- [1] Karan Ahuja, Yue Jiang, Mayank Goel, and Chris Harrison. 2021. Vid2Doppler: synthesizing Doppler radar data from videos for training privacy-preserving activity recognition. In *Proceedings of the 2021 CHI Conference on Human Factors in Computing Systems*. 1–10.
- [2] Valentina Bianchi, Marco Bassoli, Gianfranco Lombardo, Paolo Fornaciari, Monica Mordonini, and Ilaria De Munari. 2019. IoT wearable sensor and deep learning: An integrated approach for personalized human activity recognition in a smart home environment. *IEEE Internet of Things Journal* 6, 5 (2019), 8553–8562.
- [3] Federica Bogo, Angjoo Kanazawa, Christoph Lassner, Peter Gehler, Javier Romero, and Michael J Black. 2016. Keep it SMPL: Automatic estimation of 3D human pose and shape from a single image. In *European Conference on Computer Vision*. Springer, 561–578.
- [4] Tom B. Brown, Benjamin Mann, Nick Ryder, Melanie Subbiah, Jared Kaplan, Prafulla Dhariwal, Arvind Neelakantan, Pranav Shyam, Girish Sastry, Amanda Askell, Sandhini Agarwal, Ariel Herbert-Voss, Gretchen Krueger, Tom Henighan, Rewon Child, Aditya Ramesh, Daniel M. Ziegler, Jeffrey Wu, Clemens Winter, Christopher Hesse, Mark Chen, Eric Sigler, Mateusz Litwin, Scott Gray, Benjamin Chess, Jack Clark, Christopher Berner, Sam McCandlish, Alec Radford, Ilya Sutskever, and Dario Amodei. 2020. Language Models are Few-Shot Learners. arXiv:2005.14165 [cs, CL] <https://arxiv.org/abs/2005.14165>
- [5] Peipei Cao, Weijie Xia, Ming Ye, Jutong Zhang, and Jianjiang Zhou. 2018. Radar-ID: human identification based on radar micro-Doppler signatures using deep convolutional neural networks. *IET Radar, Sonar & Navigation* 12, 7 (2018), 729–734.
- [6] Xingyu Chen and Xinyu Zhang. 2023. Rf genesis: Zero-shot generalization of mmwave sensing through simulation-based data synthesis and generative diffusion models. In *Proceedings of the 21st ACM Conference on Embedded Networked Sensor Systems*. 28–42.
- [7] Jaemin Cho, Seunghyun Yoon, Ajinkya Kale, Franck Dernoncourt, Trung Bui, and Mohit Bansal. 2022. Fine-grained image captioning with clip reward. *arXiv preprint arXiv:2205.13115* (2022).
- [8] Kevin Clark, Minh-Thang Luong, Quoc V Le, and Christopher D Manning. 2020. Electra: Pre-training text encoders as discriminators rather than generators. *arXiv preprint arXiv:2003.10555* (2020).
- [9] Kaikai Deng, Dong Zhao, Qiaoyue Han, Zihan Zhang, Shuyue Wang, Anfu Zhou, and Huadong Ma. 2023. Midas: Generating mmwave radar data from videos for training pervasive and privacy-preserving human sensing tasks. *Proceedings of the ACM on Interactive, Mobile, Wearable and Ubiquitous Technologies* 7, 1 (2023), 1–26.
- [10] Jacob Devlin, Ming-Wei Chang, Kenton Lee, and Kristina Toutanova. 2019. BERT: Pre-training of Deep Bidirectional Transformers for Language Understanding. arXiv:1810.04805 [cs, CL] <https://arxiv.org/abs/1810.04805>
- [11] Shuya Ding, Zhe Chen, Tianyue Zheng, and Jun Luo. 2020. RF-net: A unified meta-learning framework for RF-enabled one-shot human activity recognition. In *Proceedings of the 18th Conference on Embedded Networked Sensor Systems*. 517–530.
- [12] Qingxiu Dong, Lei Li, Damai Dai, Ce Zheng, Zhiyong Wu, Baobao Chang, Xu Sun, Jingjing Xu, and Zhifang Sui. 2022. A survey on in-context learning. *arXiv preprint arXiv:2301.00234* (2022).
- [13] Han Fang, Pengfei Xiong, Luhui Xu, and Yu Chen. 2021. Clip2video: Mastering video-text retrieval via image clip. *arXiv preprint arXiv:2106.11097* (2021).
- [14] Chelsea Finn, Pieter Abbeel, and Sergey Levine. 2017. Model-agnostic meta-learning for fast adaptation of deep networks. In *International conference on machine learning*. PMLR, 1126–1135.
- [15] Shubham Goel, Georgios Pavlakos, Jathushan Rajasegaran, Angjoo Kanazawa, and Jitendra Malik. 2023. Humans in 4D: Reconstructing and tracking humans with transformers. In *Proceedings of the IEEE/CVF International Conference on Computer Vision*. 14783–14794.
- [16] Taesik Gong, Yeonsu Kim, Jinwoo Shin, and Sung-Ju Lee. 2019. MetaSense: few-shot adaptation to untrained conditions in deep mobile sensing. In *Proceedings of the 17th Conference on Embedded Networked Sensor Systems*. 110–123.
- [17] Xiuye Gu, Tsung-Yi Lin, Weicheng Kuo, and Yin Cui. 2021. Open-vocabulary object detection via vision and language knowledge distillation. *arXiv preprint arXiv:2104.13921* (2021).
- [18] Chuan Guo, Shihao Zou, Xinxin Zuo, Sen Wang, Wei Ji, Xingyu Li, and Li Cheng. 2022. Generating Diverse and Natural 3D Human Motions From Text. In *Proceedings of the IEEE/CVF Conference on Computer Vision and Pattern Recognition (CVPR)*. 5152–5161.
- [19] Edward J Hu, Yelong Shen, Phillip Wallis, Zeyuan Allen-Zhu, Yuanzhi Li, Shean Wang, Lu Wang, and Weizhu Chen. 2021. Lora: Low-rank adaptation of large language models. *arXiv preprint arXiv:2106.09685* (2021).
- [20] Altaf Hussain, Tanveer Hussain, Waseem Ullah, and Sung Wook Baik. 2022. Vision transformer and deep sequence learning for human activity recognition in surveillance videos. *Computational Intelligence and Neuroscience* 2022, 1 (2022), 3454167.
- [21] Md Tamzeed Islam and Shahriar Nirjon. 2020. Wi-Fringe: Leveraging text semantics in WiFi CSI-based device-free named gesture recognition. In *2020 16th International Conference on Distributed Computing in Sensor Systems (DCOSS)*. IEEE, 35–42.
- [22] Chao Jia, Yinfei Yang, Ye Xia, Yi-Ting Chen, Zarana Parekh, Hieu Pham, Quoc Le, Yun-Hsuan Sung, Zhen Li, and Tom Duerig. 2021. Scaling up visual and vision-language representation learning with noisy text supervision. In *International conference on machine learning*. PMLR, 4904–4916.
- [23] Branka Jokanovic, Moeness Amin, and Baris Erol. 2017. Multiple joint-variable domains recognition of human motion. In *2017 IEEE Radar Conference (RadarConf)*. IEEE, 0948–0952.
- [24] Jared Kaplan, Sam McCandlish, Tom Henighan, Tom B Brown, Benjamin Chess, Rewon Child, Scott Gray, Alec Radford, Jeffrey Wu, and Dario Amodei. 2020. Scaling laws for neural language models. *arXiv preprint arXiv:2001.08361* (2020).
- [25] Sagit Katz, Ayellet Tal, and Ronen Basri. 2007. Direct visibility of point sets. In *ACM SIGGRAPH 2007 papers*. 24–es.
- [26] Will Kay, Joao Carreira, Karen Simonyan, Brian Zhang, Chloe Hillier, Sudheendra Vijayanarasimhan, Fabio Viola, Tim Green, Trevor Back, Paul Natsev, et al. 2017. The kinetics human action video dataset. *arXiv preprint arXiv:1705.06950* (2017).
- [27] Gregory Koch, Richard Zemel, Ruslan Salakhutdinov, et al. 2015. Siamese neural networks for one-shot image recognition. In *ICML deep learning workshop*, Vol. 2. Lille, 1–30.
- [28] Belal Korany, Chitra R Karanam, Hong Cai, and Yasamin Mostofi. 2019. XModal-ID: Using WiFi for through-wall person identification from candidate video footage. In *The 25th Annual International Conference on Mobile Computing and Networking*. 1–15.
- [29] Yier Lin, Julien Le Kernec, Shufan Yang, Francesco Fioranelli, Olivier Romain, and Zhiqin Zhao. 2018. Human activity classification with radar: Optimization and noise robustness with iterative convolutional neural networks followed with random forests. *IEEE Sensors Journal* 18, 23 (2018), 9669–9681.
- [30] Ziyi Lin, Shijie Geng, Renrui Zhang, Peng Gao, Gerard De Melo, Xiaogang Wang, Jifeng Dai, Yu Qiao, and Hongsheng Li. 2022. Frozen clip models are efficient video learners. In *European Conference on Computer Vision*. Springer, 388–404.
- [31] Zhihan Lv, Fabio Poiesi, Qi Dong, Jaime Lloret, and Houbing Song. 2022. Deep learning for intelligent human–computer interaction. *Applied Sciences* 12, 22 (2022), 11457.
- [32] Yiwei Ma, Guohao Xu, Xiaoshuai Sun, Ming Yan, Ji Zhang, and Rongrong Ji. 2022. X-clip: End-to-end multi-grained contrastive learning for video-text retrieval. In *Proceedings of the 30th ACM International Conference on Multimedia*. 638–647.
- [33] Naureen Mahmood, Nima Ghorbani, Nikolaus F Troje, Gerard Pons-Moll, and Michael J Black. 2019. AMASS: Archive of motion capture as surface shapes. In *Proceedings of the IEEE/CVF international conference on computer vision*. 5442–5451.
- [34] Ron Mokady, Amir Hertz, and Amit H Bermano. 2021. Clipcap: Clip prefix for image captioning. *arXiv preprint arXiv:2111.09734* (2021).
- [35] Inzamam Mashood Nasir, Mudassar Raza, Jamal Hussain Shah, Shui-Hua Wang, Usman Tariq, and Muhammad Attique Khan. 2022. HAREDNet: A deep learning based architecture for autonomous video surveillance by recognizing human actions. *Computers and Electrical Engineering* 99 (2022), 107805.
- [36] Bolin Ni, Houwen Peng, Minghao Chen, Songyang Zhang, Gaofeng Meng, Jianlong Fu, Shimeng Xiang, and Haibin Ling. 2022. Expanding language-image pretrained models for general video recognition. In *European Conference on Computer Vision*. Springer, 1–18.
- [37] Alex Nichol, Prafulla Dhariwal, Aditya Ramesh, Pranav Shyam, Pamela Mishkin, Bob McGrew, Ilya Sutskever, and Mark Chen. 2021. Glide: Towards photorealistic image generation and editing with text-guided diffusion models. *arXiv preprint arXiv:2112.10741* (2021).
- [38] Hao Niu, Duc Nguyen, Kei Yonekawa, Mori Kurokawa, Shinya Wada, and Kiyohito Yoshihara. 2020. Multi-source transfer learning for human activity recognition in smart homes. In *2020 IEEE international conference on smart computing (SMARTCOMP)*. IEEE, 274–277.
- [39] Archit Parhami and Minwoo Lee. 2022. Learning from few examples: A summary of approaches to few-shot learning. *arXiv preprint arXiv:2203.04291* (2022).
- [40] Adam Paszke, Sam Gross, Francisco Massa, Adam Lerer, James Bradbury, Gregory Chanan, Trevor Killeen, Zeming Lin, Natalia Gimelshein, Luca Antiga, et al. 2019. PyTorch: An imperative style, high-performance deep learning library. *Advances in neural information processing systems* 32 (2019).
- [41] Andrea Prati, Caifeng Shan, and Kevin I-Kai Wang. 2019. Sensors, vision and networks: From video surveillance to activity recognition and health monitoring. *Journal of Ambient Intelligence and Smart Environments* 11, 1 (2019), 5–22.
- [42] Abhinanda R Punakkal, Arjun Chandrasekaran, Nikos Athanasiou, Alejandra Quiros-Ramirez, and Michael J Black. 2021. BABEL: Bodies, action and behavior with english labels. In *Proceedings of the IEEE/CVF Conference on Computer Vision and Pattern Recognition*. 722–731.
- [43] Alec Radford, Jong Wook Kim, Chris Hallacy, Aditya Ramesh, Gabriel Goh, Sandhini Agarwal, Girish Sastry, Amanda Askell, Pamela Mishkin, Jack Clark, et al. 2021. Learning transferable visual models from natural language supervision. In *International conference on machine learning*. PMLR, 8748–8763.

- [44] Alec Radford, Jeffrey Wu, Rewon Child, David Luan, Dario Amodei, Ilya Sutskever, et al. 2019. Language models are unsupervised multitask learners. *OpenAI blog* 1, 8 (2019), 9.
- [45] Hossein Raeis, Mohammad Kazemi, and Shervin Shirmohammadi. 2021. Human activity recognition with device-free sensors for well-being assessment in smart homes. *IEEE Instrumentation & Measurement Magazine* 24, 6 (2021), 46–57.
- [46] Hanooona Rasheed, Muhammad Uzair Khattak, Muhammad Maaz, Salman Khan, and Fahad Shahbaz Khan. 2023. Fine-tuned clip models are efficient video learners. In *Proceedings of the IEEE/CVF Conference on Computer Vision and Pattern Recognition*. 6545–6554.
- [47] Fatemeh Serpush, Mohammad Bagher Menhaj, Behrooz Masoumi, and Babak Karafsi. 2022. Wearable sensor-based human activity recognition in the smart healthcare system. *Computational intelligence and neuroscience* 2022, 1 (2022), 1391906.
- [48] Akash Deep Singh, Sandeep Singh Sandha, Luis Garcia, and Mani Srivastava. 2019. Radhar: Human activity recognition from point clouds generated through a millimeter-wave radar. In *Proceedings of the 3rd ACM Workshop on Millimeter-wave Networks and Sensing Systems*. 51–56.
- [49] StereoLabs. 1930. *StereoLabs AI Camera*. <https://www.stereolabs.com>
- [50] Abdulhamit Subasi, Kholoud Khateeb, Tayeb Brahimi, and Akila Sarirete. 2020. Human activity recognition using machine learning methods in a smart health-care environment. In *Innovation in health informatics*. Elsevier, 123–144.
- [51] Chi Ian Tang, Ignacio Perez-Pozuelo, Dimitris Spathis, and Cecilia Mascolo. 2020. Exploring contrastive learning in human activity recognition for healthcare. *arXiv preprint arXiv:2011.11542* (2020).
- [52] TI. 1930. *Texas Instruments*. <http://www.ti.com>
- [53] Vudit Vudit, Martin Engilberge, and Mathieu Salzmann. 2023. Clip the gap: A single domain generalization approach for object detection. In *Proceedings of the IEEE/CVF conference on computer vision and pattern recognition*. 3219–3229.
- [54] Mengmeng Wang, Jiazheng Xing, and Yong Liu. 2021. Actionclip: A new paradigm for video action recognition. *arXiv preprint arXiv:2109.08472* (2021).
- [55] Zirui Wang, Jiahui Yu, Adams Wei Yu, Zihang Dai, Yulia Tsvetkov, and Yuan Cao. 2021. Simvlm: Simple visual language model pretraining with weak supervision.
- [56] Xiaoshi Wu, Feng Zhu, Rui Zhao, and Hongsheng Li. 2023. Cora: Adapting clip for open-vocabulary detection with region prompting and anchor pre-matching. In *Proceedings of the IEEE/CVF conference on computer vision and pattern recognition*. 7031–7040.
- [57] Rui Xiao, Jianwei Liu, Jinsong Han, and Kui Ren. 2021. OneFi: One-Shot Recognition for Unseen Gesture via COTS WiFi. In *Proceedings of the 19th ACM Conference on Embedded Networked Sensor Systems*. 206–219.
- [58] Hongfei Xue, Qiming Cao, Chenglin Miao, Yan Ju, Haochen Hu, Aidong Zhang, and Lu Su. 2023. Towards generalized mmwave-based human pose estimation through signal augmentation. In *Proceedings of the 29th Annual International Conference on Mobile Computing and Networking*. 1–15.
- [59] Xianlin Zeng, Yiming Shi, and Anfu Zhou. 2022. Multi-har: Human activity recognition in multi-person scenes based on mmwave sensing. In *2022 IEEE 8th International Conference on Computer and Communications (ICCC)*. IEEE, 1789–1793.
- [60] Renrui Zhang, Rongyao Fang, Wei Zhang, Peng Gao, Kunchang Li, Jifeng Dai, Yu Qiao, and Hongsheng Li. 2021. Tip-adapter: Training-free clip-adapter for better vision-language modeling. *arXiv preprint arXiv:2111.03930* (2021).
- [61] Xiaotong Zhang, Zhenjiang Li, and Jin Zhang. 2022. Synthesized Millimeter-Waves for Human Motion Sensing. In *Proceedings of the 20th ACM Conference on Embedded Networked Sensor Systems*. 377–390.
- [62] Kaiyang Zhou, Jingkang Yang, Chen Change Loy, and Ziwei Liu. 2022. Conditional prompt learning for vision-language models. In *Proceedings of the IEEE/CVF conference on computer vision and pattern recognition*. 16816–16825.
- [63] Kaiyang Zhou, Jingkang Yang, Chen Change Loy, and Ziwei Liu. 2022. Learning to prompt for vision-language models. *International Journal of Computer Vision* 130, 9 (2022), 2337–2348.
- [64] Yunjiao Zhou, Jianfei Yang, Han Zou, and Lihua Xie. 2023. Tent: Connect language models with iot sensors for zero-shot activity recognition. *arXiv preprint arXiv:2311.08245* (2023).